Bio-Design and Manufacturing (2020) 3:396–409
https://doi.org/10.1007/s42242-020-00086-4

RESEARCH ARTICLE

Investigation of bone reconstruction using an attenuated immunogenicity xenogenic composite scaffold fabricated by 3D printing

Qiongxi Pan[1,2] · Chenyuan Gao[2] · Yingying Wang[1] · Yili Wang[2] · Cong Mao[3] · Quan Wang[3] · Sophia N. Economidou[4] · Dennis Douroumis[5] · Feng Wen[6] · Lay Poh Tan[7] · Huaqiong Li[1,2]

Received: 24 April 2020 / Accepted: 26 June 2020 / Published online: 18 July 2020

Abstract

Bone is known to have a natural function to heal itself. However, if the bone damage is beyond a critical degree, intervention such as bone grafting may be imperative. In this work, the fabrication of a novel bone scaffold composed of natural bone components and polycaprolactone (PCL) using 3D printing is put forward. α1, 3-galactosyltransferase deficient pigs were used as the donor source of a xenograft. Decellularized porcine bone (DCB) with attenuated immunogenicity was used as the natural component of the scaffold with the aim to promote bone regeneration. The 3D printed DCB-PCL scaffolds combined essential advantages such as uniformity of the interconnected macropores and high porosity and enhanced compressive strength. The biological properties of the DCB-PCL scaffolds were evaluated by studying cell adhesion, viability, alkaline phosphatase activity and osteogenic gene expression of human bone marrow-derived mesenchymal stem cells. The in vitro results demonstrated that the DCB-PCL scaffolds exhibit an enhanced performance in promoting bone differentiation, which is correlated to the DCB content. Furthermore, critical-sized cranial rat defects were used to assess the effect of DCB-PCL scaffolds on bone regeneration in vivo. The results confirm that in comparison with PCL scaffolds, the DCB-PCL scaffolds can significantly improve new bone formation in cranial defects. Thus, the proposed 3D printed DCB-PCL scaffolds emerge as a promising regeneration alternative in the clinical treatment of large bone defects.

Keywords Polycaprolactone · 3D printing · Decellularized porcine bone · Cranial bone regeneration · Attenuated immunogenicity

Introduction

Bone is generally ranked as the second most transplanted tissue worldwide. According to a recently published market report, the global market demand for bone grafts and substitutes was valued at $2.69 billion in 2017 and expected to reach the $3.91 billion by 2025 globally, with a compound annual growth rate around 4.8% in the years between 2018 and 2025 [1–3]. Bone transplantation is necessary when the defect is beyond a critical degree and the natural healing function of the tissue does not suffice to restore it. In such cases, bone grafting is the preferred option [4, 5]. Bone grafting is a surgical procedure, aiming at replacing the damaged bone with a natural or synthetic substitute. Three major types of bone grafts are commonly used: autografts, allografts, and xenografts. However, limitations pertinent to the donor supply for these methods, including the requirement of an additional surgery, donor site morbidity and limited availability instigate research endeavors for alternative sources.

Porcine bone tissue has been considered as an ideal choice for clinical xenotransplantation [6], due to its great similarities in size, physiologic compatibility with human as well as its potential for genetic modification [7]. Various

Qiongxi Pan, Chenyuan Gao and Yingying Wang have contributed equally to this work.

Electronic supplementary material The online version of this article (https://doi.org/10.1007/s42242-020-00086-4) contains supplementary material, which is available to authorized users.

✉ Lay Poh Tan
lptan@ntu.edu.sg

✉ Huaqiong Li
lihq@wiucas.ac.cn

Extended author information available on the last page of the article

studies have also shown that porcine grafts promote osteoinduction and osteoconduction [8–10]. However, a known adverse of effect of porcine tissue transplantation in primates is hyperacute rejection (HAR), caused by α1, 3-galactose (α1, 3 Gal). In this event, the enzyme α1, 3-galactosyltransferase (α1, 3 GT) synthesizes α1, 3 Gal epitopes on the cell surface. Within a few minutes or hours of contact with the blood circulation of the recipient, HAR occurs and quickly leads to the disintegration of the donor tissue. Thus, the complete removal of α1, 3 Gal from porcine tissues is a key step toward the success of xenotransplantation. In 2003, Dai and coworkers published a pioneer study on the production of α1, 3 GT deficient pigs [11]. Another research group from Massachusetts General Hospital/Harvard Medical School reported that α1, 3 GT gene-knockout swine donors in discordant xenotransplantation extended the surviving time of cardiac xenografts in baboons [12]. The study showed the absence of HAR with longer graft survival after transplantation, which is a momentous first step toward successful xenotransplantation.

Here, decellularized attenuated immunogenic bone featuring complete removal of the α1, 3-Gal epitope is used as a scaffold constituent. Decellularized bone is a widely used scaffold in bone tissue engineering [13, 14]. The ability of decellularized explants to function as natural three-dimensional scaffolds with tissue-specific orientations of the extracellular matrix (ECM) molecules, whose laboratory synthesis is troublesome, is exploited in this work. The ECM plays a central role in maintaining tissue and organ structure while preserving their organization and function [15]. It can be considered as an intricate network, composed of proteins and polysaccharides and along with resident cells and their mutual interactions regulates cell migration, proliferation and differentiation within a tissue [16]. Decellularized porcine bone ECM scaffolds are a valuable tool for bone tissue engineering reconstruction, particularly in craniofacial reconstruction where anatomically shaped bone grafts are frequently required [17].

Synthetic bone scaffolds represent another alternative bone grafting technique. Compared with auto, allo and xenografts, the major advantage of synthetic scaffolds is the unlimited donor source and the elimination of disease transmission risk [18]. However, synthetic bone scaffolds have been associated with biocompatibility, osteoinductivity and osteoconductivity issues. Poly ε-caprolactone (PCL), a bioresorbable biomaterial, is known to be nontoxic, non-immunogenic, and biocompatible [19]. The excellent biocompatibility and low toxicity of PCL make it an ideal candidate for various biomedical applications. PCL-based formulations have been approved by the FDA for clinical applications on drug-delivery systems, tissue-engineered skin, implants and prosthetic devices [20–25]. Permeability of PCL scaffolds increases when pore volume grows, which improves bone regeneration and blood vessel infiltration as well as compressive strength in vivo [26].

The need to control scaffold porosity to ascertain the development of a suitable microenvironment that will promote bone regeneration, led to the examination of 3D printing as a scaffold fabrication technique [27]. The benefits that could be harvested by the adoption of such a sophisticated method, pertain to the ability of 3D printing to manufacture complex structures in a fast and highly reproducible fashion. Moreover, the nature of the technology that uses a computationally designed model to fabricate a physical object through a single piece of equipment, the 3D printer, adds versatility to the process. Furthermore, 3D printing encompasses a wide range of technologies that enable the processing of a variety of materials, including polymer composites [17, 28, 29]. Consequently, 3D printing is rendered as an ideal candidate for the fabrication of intricate, personalized anatomically shaped bone scaffolds for individual restorations, comprised of a hybrid composite material. Therefore, the main objective of this research is the development of a composite bone scaffold for bone defect reconstruction, composed of xenogeneic bone with attenuated immunogenicity and polymer, and fabricated using 3D printing. In the framework of this study, a series of systematic investigations of the scaffold structure was conducted, along with a thorough examination of the physicochemical and in vitro biological properties of the 3D printed DCB-PCL composite scaffolds. Finally, an in vivo critical size rat cranial defect model was created to observe the effect of the scaffolds in bone formation.

Materials and methods

Decellularized bone tissue

Subchondral trabecular bone was extracted from pigs. A high-pressure water jet was applied to remove the marrow. The bones were then purged in phosphate-buffered saline (PBS) containing 10 mM Tris (Sigma-Aldrich) for 24 h at room temperature. Next, they were rinsed in PBS, followed by decellularization in trypsin 0.25% w/v for 24 h at 37 °C. The bones were washed for 1 h in PBS, followed by another washing cycle in PBS with 10 mM Tris and 0.1% sodium dodecyl sulfate (SDS; Sigma-Aldrich), for 1 day at room temperature. Extensive PBS washes were implemented to remove the SDS, followed by submersion in PBS containing 10 KIU/ml aprotinin (Roche Applied Science), 1 ug/mL leupeptin (Roche Applied Science), 1 mM PMSF (Sigma-Aldrich) and 0.1% w/v EDTA (Sigma-Aldrich) for 1 h at 37 °C. Afterward, the enzymes were removed with extensive washes in PBS and the processed bones were washed in water and stored via lyophilization. A cryo-mill (Retsch, Germany) was used here to

pulverize the decellularized trabecular bones, with a frequency of 10 cycles per second for 15 min, to obtain bone particles. Lastly, the particles were passed through a 40 μm cell strainer twice, to ensure that their size did not exceed 40 μm, aiming at minimizing the risk of particle aggregation and clogging of the printer nozzle.

Characterization of decellularized bone tissue

Scanning electron microscopy (SEM) was used to visualize the bone tissue after decellularization and perform statistical analysis of the particle size of the decellularized bone powder by the software Image J. A tissue DNA kit (E.Z.N.A®, Omega Bio-tek) was employed to extract total genomic DNA from the samples, which was measured with a micro-volume UV–Vis spectrophotometer (Thermo Scientific NanoDrop One, Queensland). The samples and respective measurements were in quadruplicates. H&E staining as well as Masson staining was carried out to characterize the composition of DCB. Briefly, the DCB constructs were retrieved from the bone tissue after decellularization, cleaned with PBS thrice and then restored in 2.5% glutaraldehyde (Beijing Chemical Plant, China). Afterward, H&E (C0105, Beyotime Biotechnology China) staining and Masson trichrome staining (Cyagen, China) were added to the samples according to the manufacturers' instructions. Images were then captured with an optical microscope (Ni-U-5000, NIKON, Japan).

Preparation of the composite scaffolds via 3D printing

PCL with a molar mass of 43,000–50,000 g/mol (Sigma-Aldrich) and DCB powder were freeze-dried to prevent the occurrence of hydrolysis and oxidative degradation. The process of mixing the PCL and DCB powders was carried out in a 60 °C laboratory environment, using a co-rotating twin-screw mini extruder (DSM Xplore 15 ml Micro-compounder), which resulted in DCB-PCL composite filaments of 1.7 ± 0.5 mm in diameter. 3D-printing of PCL and DCB-PCL porous scaffolds was performed using a MakerBot Replicator desktop 3D printer (MakerBot Inc., USA). The printer was equipped with a nozzle of 350 μm in diameter. The printing parameters were set for standard resolution without the raft option being activated. After the 3D printing was completed, the samples were sonicated for 30 min in an ultrasonic bath, to remove residual surface particles and ledges and to obtain regular shaped scaffolds.

Compressive and tensile testing of the composite materials

Compressive testing on cylindrical scaffolds ($r = 0.5$ cm, $h = 0.5$ cm) was conducted using a microcomputer controlled electronic universal testing machine (WDW-0.5C, Shanghai Hualong Microelectronics Co. Ltd., China) with a compression speed of 2 mm/min. Tensile fatigue testing required the material to be molded into dog-bone-shaped samples (3 mm thick and 5 mm wide at the center). Axial force tensile testing with a speed of 10 mm/min (WDW-0.5C, Shanghai Hualong Microelectronics Co. Ltd., China) was performed, till sample fracture.

Rheology testing of the composite materials

Rheology analysis was conducted using a stress-controlled rheometer (TA Instruments, DHR-2, 5000), equipped with a Peltier stage. The samples were prepared into PTFE molds as 8-mm-diameter and 1-mm-thick wafers. A TA Discovery Series HR-1 Rheometer, equipped with an 8 mm parallel plate fixture, was employed to perform oscillatory frequency sweep tests (1–100 Hz, 1% strain at 37 °C). Storage (G') and Loss moduli (G'') data were recorded throughout the tests.

FTIR and Raman spectroscopy

Real-time Fourier-transform infrared spectroscopy (FTIR, BRUKER, Tensor II 5000, German) was applied to monitor the combination of DCB and PCL using 3D printing. The FTIR spectra were collected from 500 to 4000 cm^{-1} with a 2 cm^{-1} resolution and were used to compare the structural differences between pure DCB and PCL. Raman spectroscopic analysis was performed with a confocal Raman microscope (inVia Renishaw, UK) coupled with a spectrograph with a diffraction grating of 600 lines/mm.

SEM and EDS analysis

SEM micrographs of the porous scaffolds were taken after 3D printing. The scaffolds were coated with Au and their morphologies were observed with a field-emission scanning electron microscope (FESEM; SU8010-5000, Hitachi, Japan) at a 5.0-kV accelerating voltage. At the accelerating voltage of 20 kV, their chemicals were presented by introducing energy dispersive spectrometry.

Accelerated scaffold degradation in vitro

To accelerate the hydrolysis reaction, sodium hydroxide (5 M NaOH) was used. Each scaffold (10 mm × 10 mm × 8 layers) was soaked in a tube, which contained 10 ml NaOH and was covered by a tightened screw cap. The tube temperature was maintained at 37 °C. To perform the analyses, the PCL scaffolds were removed weekly at a time point (0–6 weeks), while the DCB-PCL scaffolds sub-daily, at a time point (up to 2.5 days). Upon removal from the tubes,

the scaffolds were thoroughly rinsed with deionized water and then dried in an oven at 35 °C for 12 h.

In vitro cell culture

American Type Culture Collection (ATCC) provided us with human mesenchymal stem cells (hMSCs), which were grown in 75 cm^2 cell culture flasks in Mesenchymal Stem Cell Basal Medium (MSCBM, ATCC) with the supplementary Mesenchymal Stem Cell Growth Kit (ATCC). All experimental procedures were done using cells from passage 4 to passage 6 in a controlled environment of 37 °C humidified atmosphere with 5% CO_2 and 95% air.

Ultraviolet light was used to sterilize all the testing scaffolds. A direct seeding of the scaffolds was done with a 100 ml aliquot of hMSCs suspension containing 1×10^5 cells. Then 4 h pre-adhesion followed with addition of DMEM culture medium (GIBCO) supplemented of 10% fetal bovine serum (FBS, GIBCO). The plates were kept under humidified culture conditions.

Cell viability of hMSCs

Under the manufacturer's instructions (LIVE/DEAD Viability/Cytotoxicity Kit, Molecular Probes, USA), a harvest and growth-medium incubation of scaffolds required a period of 21 days and 30 min of darkness in 2 μM calcein AM (for live cells staining) and 4 μM ethidium homodimer-1 (for dead cells staining). Then, the stem cells on the scaffolds were carefully rinsed with PBS. The fluorescence was finally visualized after washing with PBS thrice, using an inverted fluorescence microscope (Leica, DMi8).

Alkaline phosphatase (ALP) activity of hMSCs

We measured the ALP activity at 7 and 14 days, respectively, to assess the osteoblastic differentiation of the hMSCs that were grown on the scaffolds. Specified samples ($n = 3$ at each time point) were used to take the DNA quantitative measurements, doing a 45-min lysing of cells via sonication at room temperature in a solution of 1 mL of 0.02 wt% triton-X 100 (Bio-Rad) in DNA-free water. Based on the manufacturer's instructions, we employed a Quanti-iT™ Picoreen® dsDNA Assay Kit (Invitrogen) to quantify double stranded DNA within cell lysates via fluorescent assay. Moreover, the alkaline phosphatase activity was determined via an ALP activity kit (Beyotime Biotechnology, P0321). Normalization was processed through both ALP activity values and their corresponding sample-specific dsDNA ones.

Real-time polymerase chain reaction (RT-PCR) analysis

qRT-PCR was employed to measure the osteogenic expression of genes such as runt-related transcription factor 2 (RUNX2), bone sialoprotein (BSP), alkaline phosphatase (ALP), osteocalcin (OCN) and osteopontin (OPN). 7 days later, the Trizol reagent was used to extract the total RNAs of stem cells on scaffolds. With the PrimeScript RT reagent kit and under its manufacturer's instructions, the RNA purity was examined by NanoDrop (DeNovix), while the 1st strand of complementary DNA (cDNA) was reversed to transcribe from RNA. Quantitative PCR was done in a total volume of 20 μl with selected primers (shown in Table 1) and the SYBR Green PCR Kit (TAKARA). The $2^{-\Delta\Delta Ct}$ method was used for data analysis, while β-Actin was considered as the housekeeping gene. The normalized results were recorded by the operator, as the mean values of the corresponding control groups.

Animal experiments

Twenty mature male Sprague–Dawley (SD) rats (mean body weight between 250 and 300 g), fed on sterilized food and water, were bedded in cages with a 12-h light/dark switch cycle. The animals were randomly separated into two groups. The rats were anesthetized after an intraperitoneal injection of chloral hydrate (10%; 0.4 mL/100 g body weight) under sterile conditions. A 1.5 cm sagittal incision was made in each animal's scalp. Blunt dissection was applied to expose the calvarium, while a dental trephine was used to create two critical-sized cranial defects with a 6 mm bilateral diameter, into which the scaffolds were implanted. Subsequently, after injection of an intramuscular antibiotic, the animals were left free to eat food and drink water, while monitored

Table 1 Primer sequences used for the RT-qPCR analysis

Gene symbol	Forward primer (5′–3′)	Reverse primer (5′–3′)
BSP	TGTCTGCTGAAACCCGTTC	GGGGTCTTTAAGTACCGGC
OCN	GTGACGAGTTGGCTGACC	TGGAGAGGAGCAGAACTGG
OPN	CTCCATTGACTCGAACGACTC	CAGGTCTGCGAAACTTCTTAGAT
ALP	GTATCGGCAGCAGTCAGCAGTG	TCCAGGCAGGCGGCGAAG
RUNX 2	TTCCAGACCAGCAGCACTC	CAGCGTCAACACCATCATTC
β-actin	CATGTACGTTGCTATCCAGGC	CTCCTTAATGTCACGCACGAT

daily for potential complications. The rats were then sacrificed with an overdose of anesthetic at the 4th, 16th and 20th week post-operation and their craniums were harvested and kept in a 4% paraformaldehyde solution, containing 0.1 M phosphate solution (pH 7.2), overnight prior to experimentation.

Micro-computed tomography (micro-CT)

Calvarias were collected after euthanasia of 3 animals at the 4th, 16th and 20th post-operative week, respectively, and were stored in 4.5% neutral buffered formalin for 12 h. The samples were observed with micro-CT (Skyscan 1174, Bruker). The micro-CT system software package was employed to convert the final reconstructed data to three-dimensional images.

Statistical analysis

The data collection was completed in three separate experiments, which were processed to generate the mean and standard deviation values. The one-way ANOVA and Tukey procedure post hoc tests were introduced to determine the level of significance, p values < 0.05 being considered as significant.

Results

Characterization of decellularized bone tissue and powder

The decellularized bone powder was prepared using cryomilling as described earlier. The morphology of the decellularized bone tissue after milling is shown in Fig. 1a. It can

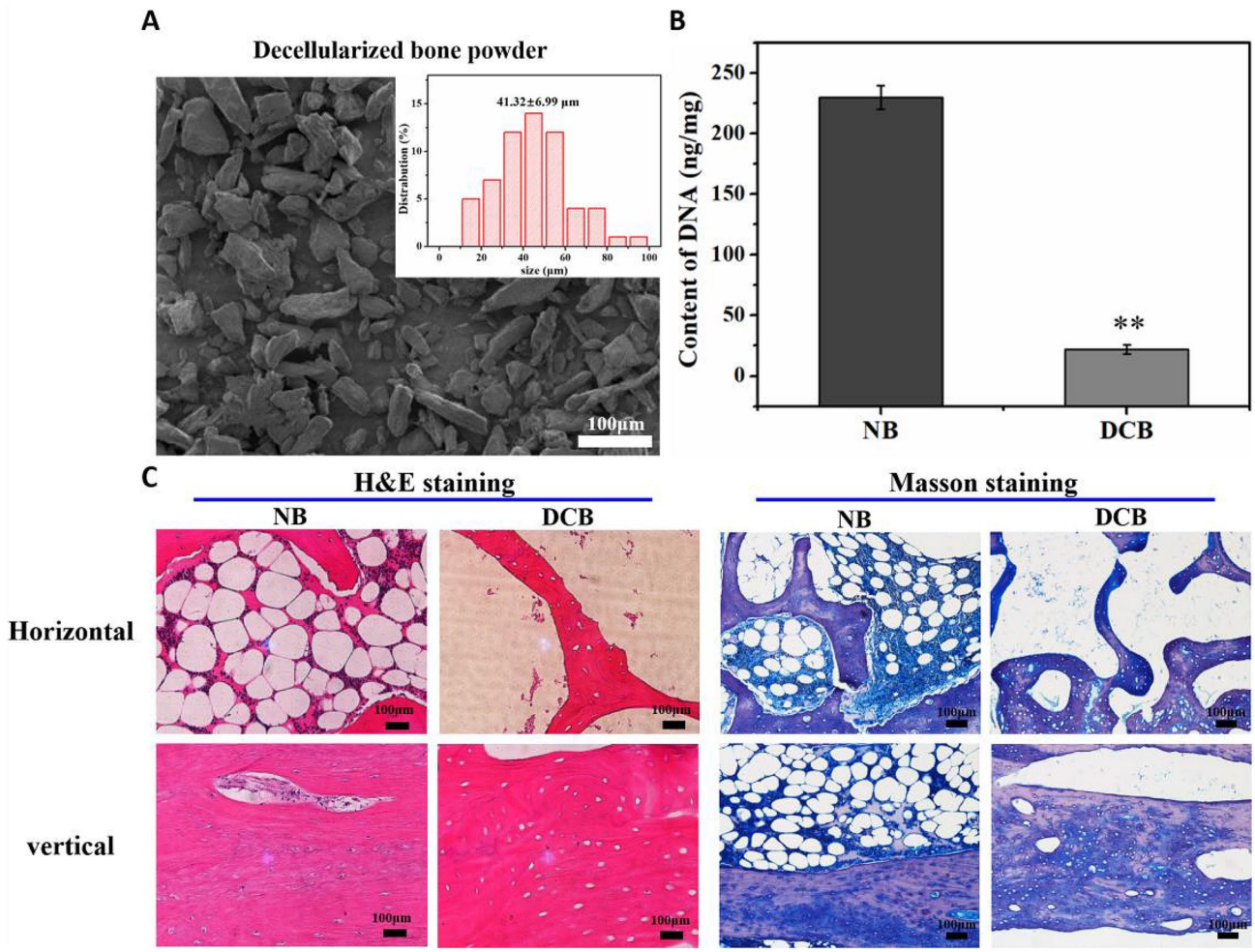

Fig. 1 Characterizations of bone tissue before and after decellularization. **a** SEM images of the decellularized bone tissue (DCB); **b** quantification analysis of DNA amount in NB and corresponding DCB; **c** H&E staining and Masson's Trichrome Staining for cell nuclei and extracellular matrix corresponding to DCB. Highly significant $^{**}p < 0.01$

be seen that the powder particle size is around 40 μm or less. We carried out both quantitative (Fig. 1b) and qualitative (Fig. 1c) examinations of the decellularization efficiency. As shown in Fig. 1b, the content of DNA was significantly reduced after decellularization. Images illustrated in Fig. 1c confirmed the success of decellularization via Histological H&E and Masson's Trichrome Staining for nuclei and extracellular matrix. From H&E staining, nuclei in the native bone (NB) tissue exhibited blue staining distributed homogeneously throughout the tissue while blue staining was completely absent in the matrix after decellularization, signifying the efficient removal of cells during the decellularization process. However, eosin staining remained, revealing the good preservation of major extracellular components in DCB. The result of Masson's Trichrome Staining also confirmed the retention of most of the main constituents of the extracellular matrix. The morphology was also observed to be almost the same before and after decellularization, which was in accordance with the H&E staining results.

Physicochemical properties of DCB-PCL composites

The DCB-PCL composites were fabricated with varying DCB content and molded into disks for further characterization. In Fig. 2a, it is shown that the color of the composite scaffolds gradually deepened with the increase in decellularized bone powder percentage. The samples were subjected to mechanical testing in both the compressive and tensile modes (Fig. 2b, c). It was found that the compressive modulus increased with increasing DCB content, up to 175 MPa, for 20% DCB. Nonetheless, at the addition of 50% DCB, the modulus dropped to 110 MPa. Regarding the tensile modulus, there is no apparent trend correlated with the addition of DCB.

Rheological characterization is crucial for extrusion-based processes, such as the FDM printing technique. As shown in Fig. 2d, the addition of DCB generally increases the viscosity. At 50% DCB, the initial viscosity was increased by approximately 12 times, compared to pure PCL. However, the onset of shear thinning appeared at lower shear rates for 30 and 50% DCB.

FTIR and Raman spectroscopy (Fig. 2e, f) were employed to confirm the availability of the decellularized ECM component on the surfaces of DCB-PCL. The former showed the characteristic peaks of PCL and DCB in the hybrid group, and no new absorption peaks were found. On the other hand, the Raman spectrum of a printed sheet of 30% DCB, presented an absorption peak at 960 cm^{-1} corresponding to the phosphate component of bone and another at 1660 cm^{-1} corresponding to the amide signal I of collagen [30]. Both of the two peaks, also appearing in the Raman spectrum of native trabecular bone, were clearly presented in our DCB composite spectrum but not in that of pure PCL, which is consistent with previous observations reported [31]. The meaningful results in the PCL phase cover 3 peaks: the triple peak centered around 1450 cm^{-1} for δ_{CH2} (fourth carbon from the carbonyl), the double one at 1300 cm^{-1} for ω_{CH2} (furthest carbon from the carbonyl) and the skeletal

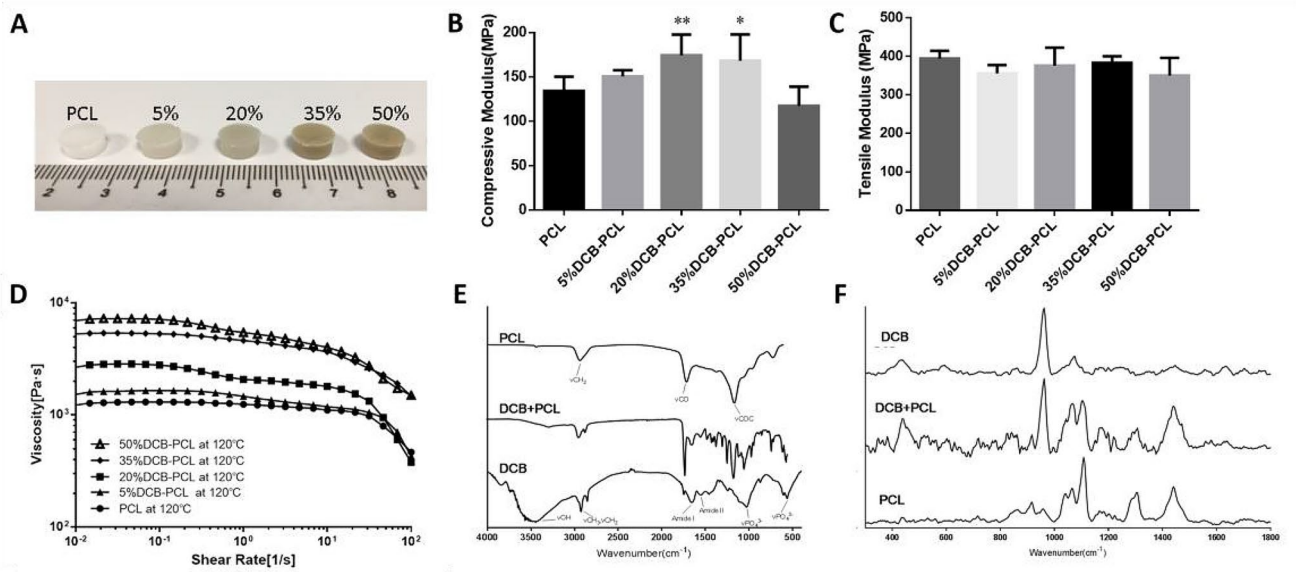

Fig. 2 Physicochemical Characterization of DCB-PCL composites. **a** Macroscopic observation of different concentrations of DCB, featuring 5%DCB-PCL, 20%DCB-PCL, 35%DCB-PCL and 50%DCB-PCL scaffolds; **b** and **c** Compressive and tensile modulus of PCL and DCB-PCL scaffolds; **d** rheological test of different concentration scaffolds; **e** FTIR of pure and hybrid material; **f** Raman spectroscopy of PCL and composite material ($n=6$; *indicated significant differences, $p<0.05$; **indicated highly significant differences, $p<0.01$.)

stretching at 1110 cm^{-1} [31, 32], the signals of which appear both in the spectrum of PCL and composite samples.

Characterization of 3D printed porous composite scaffolds

Through the 3D printing technology, we obtained homogeneous porous 3D printed DCB-PCL composite scaffolds. SEM images (Fig. 3a, b) showed that all DCB-PCL scaffolds have similar architecture, i.e., regular macroporous structure. Magnified images of cross-sectional surfaces are shown in Fig. 3c. As depicted, the macroporous structure, formed by uniform square pores, is characterized by pore size and porosity of about 700 μm and 60%, respectively. It is also clearly illustrated that visible pores were present at DCB concentration of 20% onwards. The higher content of DCB powder also induced a rougher surface compared to the PCL samples. From the EDS analysis (Fig. 3d–h), the calcium and phosphorus elements were clearly present in the DCB-PCL scaffolds as expected and when quantified (Fig. 3i), the detected mass percentage of the elements increased with increasing DCB concentration accordingly.

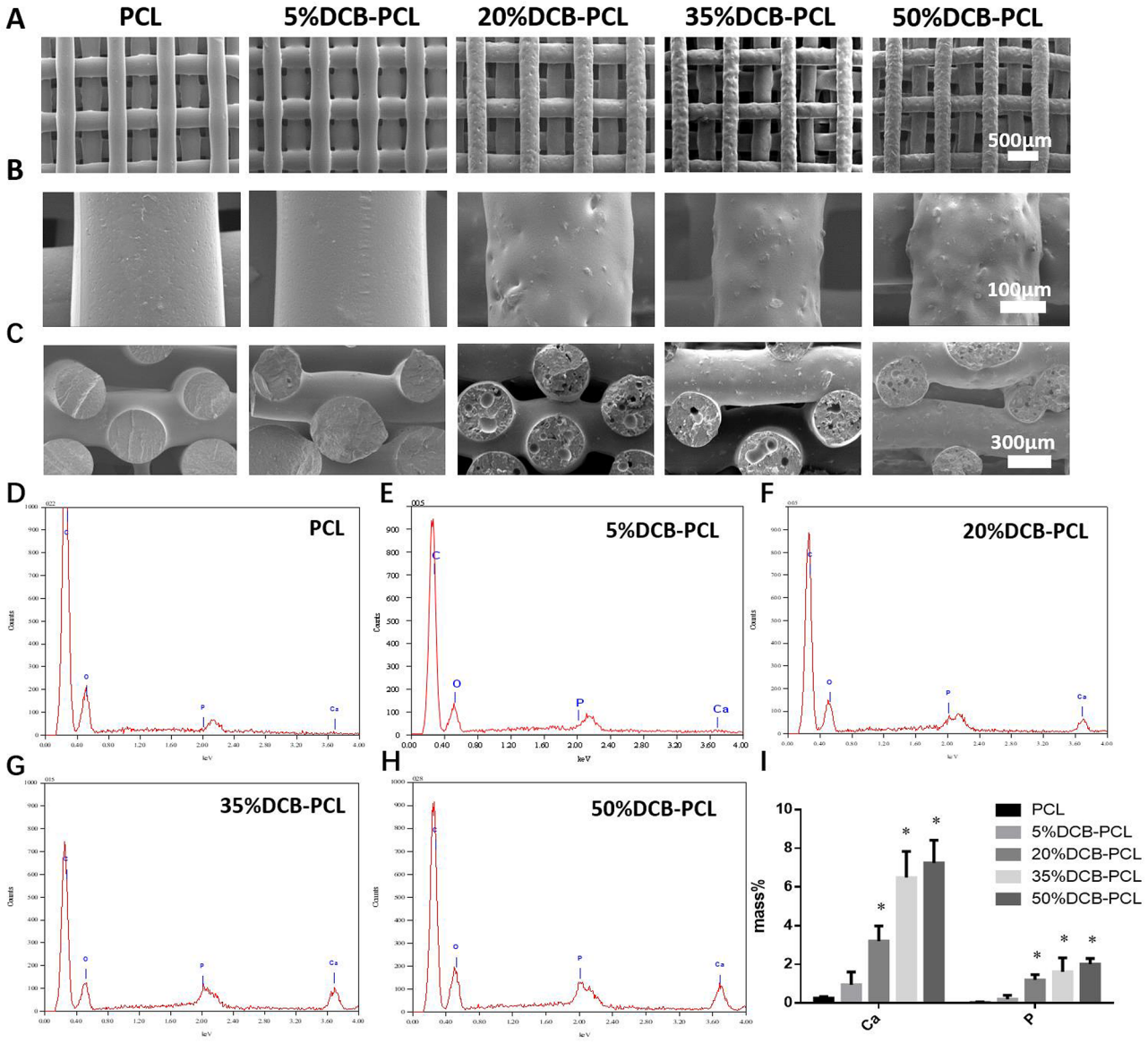

Fig. 3 **a** and **b** SEM observations of PCL, 5%DCB-PCL, 20%DCB-PCL, 35%DCB-PCL and 50%DCB-PCL scaffolds at different magnifications, respectively; **c** Cross-sectional SEM images of PCL and 50%DCB-PCL; **d**–**h** EDS analysis of surfaces of all the scaffolds; **i** Ca and P contents in scaffolds of different concentrations (*Indicated significant differences, $p < 0.05$)

Degradation of 3D printed DCB-PCL and PCL scaffolds

The studies above confirm that DCB has been successfully incorporated and printed into scaffolds. The mechanical characterization initially showed an improvement of the mechanical performance under compression and tension, analogous to the increasing DCB content; however, the mechanical properties declined for 50% DCB. Therefore, for further studies, only DCB concentrations of up to 35% will be investigated.

PCL is well known for its fairly slow degradation rate that can last for up to 4 years in certain conditions. Results generated from several studies [31, 32] indicate that hydrolytic random scission is mainly employed as the major degradation mode for high molecular weight aliphatic polyesters, while biodegradation seems only to apply to lower molecular weight by-products (Mn < 5000) or sub-micron sized particles which are possibly recognizable and ingestible for phagocytes. An acidic or basic medium was used to achieve accelerated degradation, in an aim to enhance the hydrolysis of polyesters; besides, compared with other relevant methods, such as temperature acceleration, the accelerated degradation would be better suited to mimic physiological conditions. Relevant studies on polymeric films and devices report the use of alkaline mediums [33]. While PBS would be a suitable medium as it would simulate the in vivo physiological conditions, studies have shown that after 60 months, the average loss of the PBS-degraded PCL scaffolds reached about 18% [34]. Consequently, in this study we employed an alkaline medium (5 M NaOH) to carry out the accelerated degradation studies of PCL and PCL-based composite scaffolds.

As shown in Fig. 4a, all the DCB-PCL scaffolds showed different degrees of degradation within 48 h with DCB at 35% showing the highest mass loss, followed by 20% and 5%. The PCL scaffold was the most stable and no significant mass loss was observed within the 48 h of study. An extended study of up to 5 weeks was carried out for the PCL scaffold, whereby complete degradation was observed (Fig. 4b).

Cellular responses to 3D printed DCB-PCL scaffolds

In vitro experiments aimed at evaluating the regeneration potential and supportive capability of 3D printed DCB-PCL scaffolds (Fig. 5) for human mesenchymal stem cell (hMSCs) adhesion and viability till day 21. The cells were observed to proliferate well, with a uniform distribution over the entire scaffold. The absence or negligible numbers of dead cells were reported, as verified by the absence of red stain. Thus, both PCL and DCB-PCL scaffolds could efficiently support stem cell viability and proliferation.

Without introducing any osteogenic medium for hMSCs cultured on 3D printed DCB-PCL scaffolds, osteogenic differentiation studies were further conducted using qPCR (Fig. 6). Cell differentiation was evaluated by the expression of selective osteogenic markers RUNX2, BSP, OPN, ALP, and OCN at the 7th and 21st days (Fig. 6a–e). The RUNX2 and BSP gene markers increased by 1.5-fold as the DCB content was increased from 5 to 35%. Moreover, the OPN marker increased by 2.5-fold for the 20% DCB scaffolds and reached a fivefold increase for 35% DCB content. On the other hand, the ALP and OCN markers increased by almost sevenfold at day 21 for 35% DCB. As a result of the gene expression analysis presented, once DCB is incorporated into PCL scaffolds, the osteogenic differentiation of hMSCs could be promoted. With the increase in the culturing period, expression of all the osteogenic genes was regulated upon

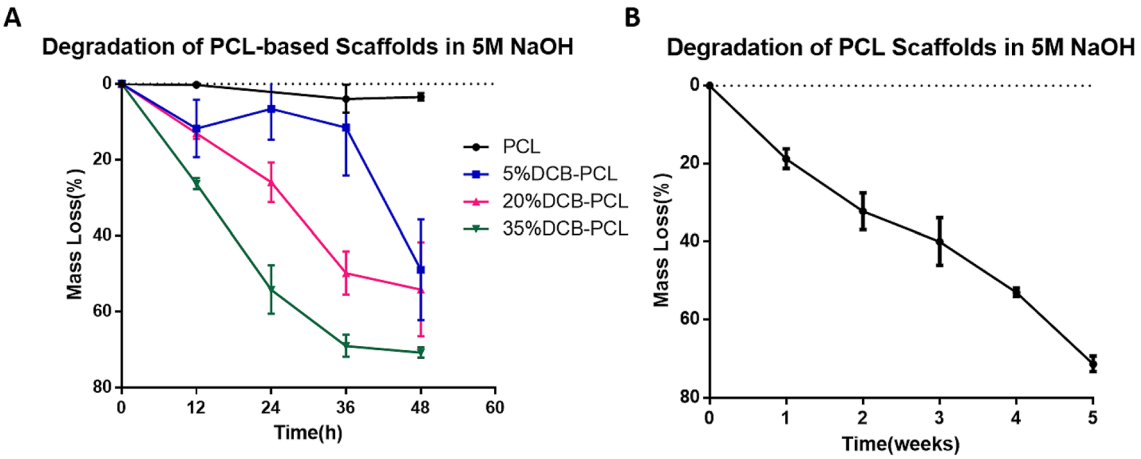

Fig. 4 Degradation of scaffolds over time. **a** Percentage of mass loss of DCB-PCL scaffolds over 48 h; **b** Percentage of mass loss of PCL scaffolds over 5 weeks

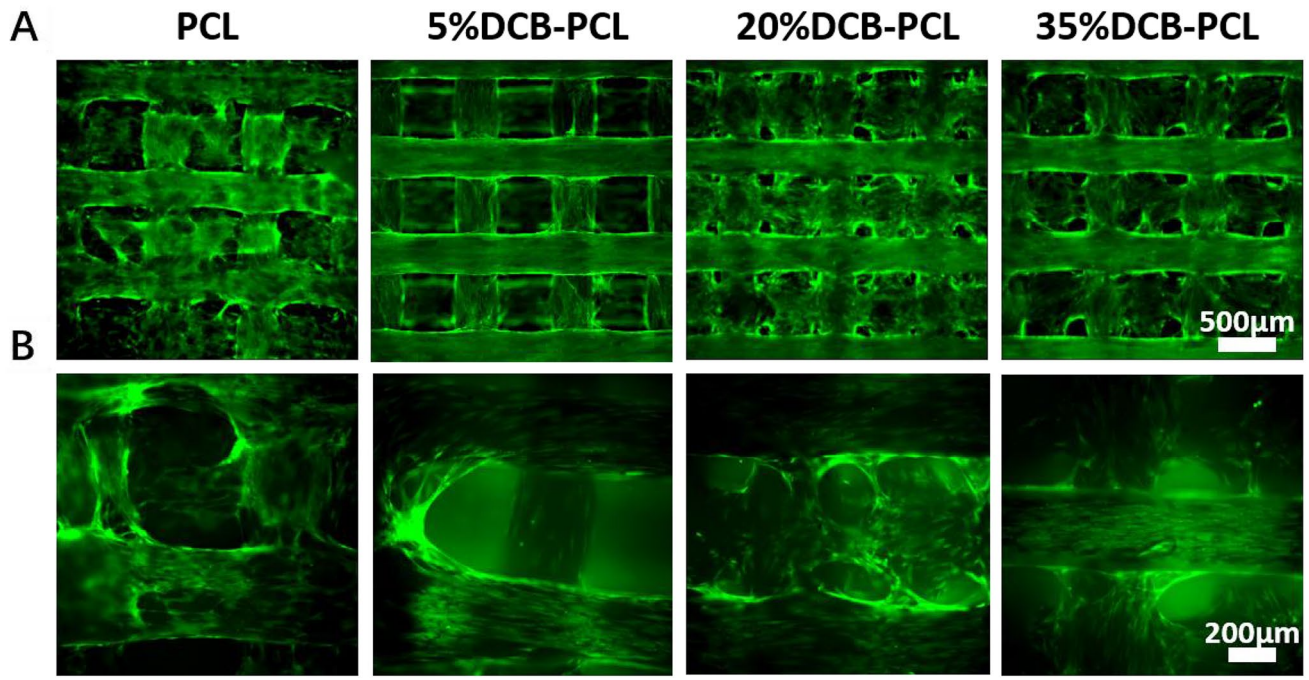

Fig. 5 Laser-scanning confocal reconstructions of live (green; calcein AM) and dead (red, ethidium homodimer-1) stains of hMSCs on day 21 at different magnifications, respectively; Scale bar indicates **a** 500 μm and **b** 200 μm

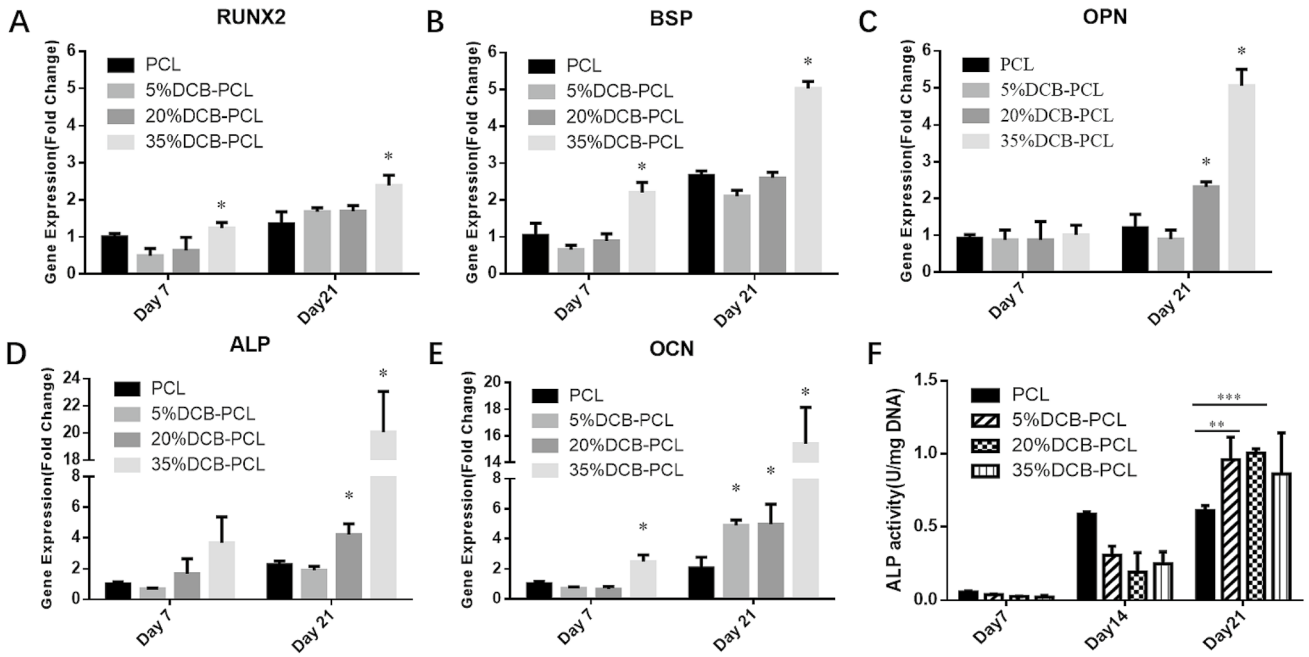

Fig. 6 Osteogenic expression of **a** RUNX2, **b** BSP, **c** OPN, **d** ALP and **e** OCN for hMSCs cultured on the PCL, 5%DCB-PCL 20%DCB-PCL and 35%DCB-PCL scaffolds through qRT-PCR analysis after 7 and 21 days, respectively ($n=3$; *indicated significant differences in comparison with PCL, $p<0.05$). **f** ALP activity of hMSCs cultured for 7, 14 and 21 days, respectively, on the PCL, 5%DCB-PCL 20%DCB-PCL and 35%DCB-PCL scaffolds (**indicated significant differences in comparison with PCL, $p<0.01$; ***indicated significant differences in comparison with PCL, $p<0.001$)

the DCB-PCL scaffolds. Comparatively, the 35%DCB-PCL scaffolds manifested enhanced expression levels.

Alkaline phosphatase (ALP) activity, an early signal of osteogenesis, increased substantially at the initial period of up to 14 days of culture, but no further increase was observed at 21 days for the cells on PCL scaffolds (Fig. 6f). In contrast, the cells on 5%DCB-PCL, 20%DCB-PCL and 35%DCB-PCL scaffolds all exhibited a steady increase. This is probably attributed to the fact that the proliferation ability of cells reached the peak on the 14th day. Then, when the proliferation ability of cells gradually began to weaken, the differentiation ability was enhanced. Therefore, after the 14th day, the ALP secretion ability of the composite scaffolds containing DCB was higher than that of the pure PCL scaffolds.

Bone regeneration in cranial defects

The results generated by the in vitro experiments demonstrated that the 35% DCB-PCL composite scaffold had promising effects on viability and osteogenic differentiation of stem cells. Therefore, the 35% DCB-PCL scaffold was further studied for the in situ bone defect experiment in vivo, with the PCL scaffold employed as control. Cranial bone defects (=6 mm) were formed in the cranium of SD rats and the PCL and 35%DCB-PCL scaffolds were trimmed to fit well into the circular bone defect. All the animals survived surgery.

Figure 7 presents the 3D morphology of the repaired cranial bones at the 4th, 16th and 20th week, as imaged by micro-CT. Initially, the micro-CT analysis was carried out to assess the 3D structure of the repaired cranium. At the 4th post-operative week, new bone formation scarcely occurred at the defect site within the PCL control sample (Fig. 7a1), while no treatment was applied. Obvious one-piece new bone formation was detected in the experimental group treated with the 35%DCB-PCL scaffold, while the surrounding host bone tissue and the defect area was still recognizable in the control group (Fig. 7a1–a2). At the following 16th and 20th weeks, with the lengthening of rat survival time, the osteogenesis at the defect area was fairly poor in the control sample, shown by a visible hole located at the center of the defect area (Fig. 7a3, a5), with the exception of dot bones sprouting. The detection of the defect is facilitated by its contour, which signifies minimal bone self-healing for the 6 mm defect during the period of experiment. Nonetheless, both the 35% DCB-PCL scaffold-treated groups and newly regenerated bone fragments were found in the defect areas (Fig. 7a4, a6). The quantitative results of the newly formed bone within the defect confirmed the above-mentioned studies. Moreover, the micro-CT measurements indicated that the values of both bone mineral density and volume per total trabecular volume were significantly higher in the biohybrid of DCB and PCL scaffold groups than in the PCL groups (Fig. 8). It is noteworthy that the bone growth was minimal and not clearly obvious at the defect sites of the PCL group during the whole experimental time. However,

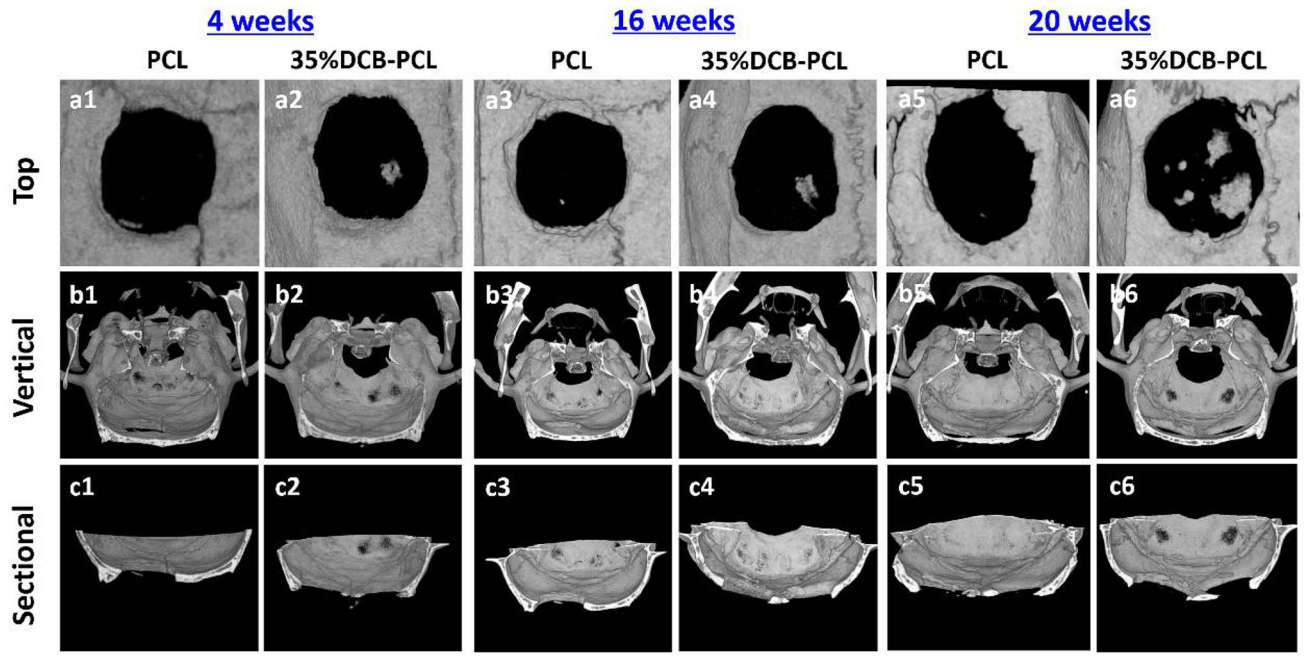

Fig. 7 Representative 3D micro-CT photographs of the regenerated rat cranial bone defects with PCL group and 35%DCB-PCL group at the 4th (**a1**–**c1** and **a2**–**c2**),16th (**a3**–**c3** and **a4**–**c4**) and 20th week (**a5**–**c5** and **a6**–**c6**) post-operation

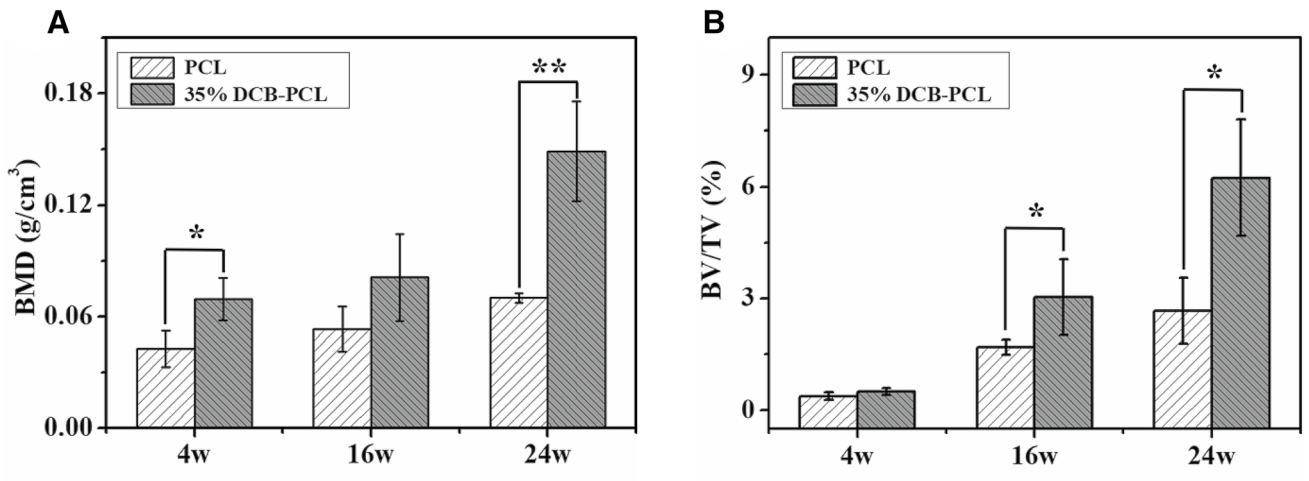

Fig. 8 Quantitative micro-CT analysis of **a** bone volume and **b** bone volume within the defect for PCL group and 35%DCB-PCL group. $*p < 0.05$, $**p < 0.01$

the 35%DCB-PCL group achieved the increase in new bone formation, which is owed to the incorporation of DCB in the PCL scaffolds.

Discussion

Despite the recent progress in regenerative medicine, the repair of critical size bone defects remains a major clinical challenge due to serious complications of trauma, inflammation, and tumor surgery. Our study succeeded in creating porous DCB-PCL scaffolds via 3D printing. Components in natural bone play an important regulatory factor to initiate bone regeneration, and 3D printed scaffolds composed of xenogenic bone components and synthetic polymer expedited the bone regeneration process in vivo. Bone chips are considered as the best candidate to induce bone regeneration [35] and their use in this study demonstrated their potential as constituents of a sophisticated 3D printed scaffold. The use of xenogenic bone with attenuated immunogenicity in xenotransplantation emerges as a key tool toward the success of xenotransplantation.

Here, we explored the decellularization of bone chips and their incorporation in the material for scaffold fabrication. After decellularization, most of the ECM components could be retained and cells including nucleus or genetic materials were completely eliminated (Fig. 1). After cryomilling, the DCB was blended with PCL to yield the base materials for 3D printing. Since the US Food and Drug Administration (FDA) approved the use of PCL due to its excellent biocompatibility, PCL has been widely employed for clinical applications [21–24, 36]. The implementation of 3D printing technology allowed the precise control of pore size while the morphology within the printed PCL and composite scaffolds was accomplished. As it is known, the natural bone consists of trabecular bone encircled by cortical bone, which creates a porous environment characterized by 50–90% porosity and 1 mm pore size [37, 38]. Only when the microenvironment of the trabecular bone in respect of the respective cell–cell/cell–matrix interaction [38] (Fig. 3) is imitated, a bone scaffold can be considered ideal. In general, high pore volume facilitates the permeation of nutrients into the scaffold, and thus enhances cell proliferation and blood vessel infiltration as well as internal mineralized bone formation [39]. Hence, the 3D-printed DCB-PCL scaffolds proposed in this study exhibit similar desirable macroporous structure, meeting the criteria to favor bone regeneration.

In regard to the mechanical behavior of the composite scaffolds, matching their stiffness with the respective of the adjacent bone was a critical parameter considered during the design process. This was done to avoid the 'stress shielding effect', wherein the mismatch of stiffness between implant and bone may result to insufficient loading of the bone tissue and eventually osteopenia [40]. Hence, we aimed to approximate the compressive properties of the natural bone, given that the defected cranium area is most likely to be subjected to compressive loading. According to the related literature, the compressive modulus of human cancellous bone is about 12-140 MPa [41]. The undertaken mechanical tests (Fig. 2) indicate that the compressive modulus was within the range of 130 to 180 MPa, increasing with the respective increase in DCB concentration from 5 to 35%. These findings show that the compressive stiffnesses of the DCB-PCL scaffolds was arithmetically in close proximity to the respective of natural bone. It is also noteworthy that the bioactive PCL can trigger the precipitation and growth of hydroxyapatite (HA), the main component of DCB, so it can be used as a

binder between the scaffold and bone tissue to promote bone regeneration. [42]

The cell–material interaction has considerably influenced the stem cell adhesion, migration, proliferation and differentiation, which are all key occurrences before bone is mineralized [43, 44]. In the present study we investigated all the above, including the adhesion, viability, ALP activity and osteogenic gene expression of hMSCs, cultured on the composite scaffolds. DCB-PCL scaffolds induced a continuous stimulation of the ALP activity and osteogenic commitment of hMSCs with increasing DCB addition in the absence of induction medium. Decellularized bone contains natural extracellular matrix, which offers a structural support to cells for cell growth and naturally stored cytokines within the bone matrix to drive bone tissue formation [13].

The role of DCB-PCL scaffolds in bone regeneration in vivo was evaluated by testing their ability to repair critical size cranial defects in a rat model. When implanted in the cranial defect, the scaffolds were in an inert state due to insufficient blood supply and relative lack of bone marrow in the cranium. Micro-CT images revealed enhanced osteogenesis in a cranial defect model using 35%DCB-PCL scaffolds. This is a result of the DCB containing many active ingredients that promote bone differentiation. DCB-PCL scaffolds enhanced new bone formation in a statistically significant manner, with improved efficacy with increasing DCB content. The efficacy of the DCB-PCL scaffolds is clearly demonstrated in comparison with the control PCL scaffold group, where little or none new bone formation was reported in the defect areas, within the time frame studied (Fig. 7). Moreover, the quantitative data (Fig. 8) of BMD and bone volume per total volume illustrated that the DCB-PCL scaffolds induced an enhanced osteogenic effect.

It is evident that the addition of DCB in the PCL scaffolds provided an advantageous bone extracellular microenvironment, while satisfied the need for faster scaffold degradation rates with simultaneous new bone formation, attributed to a comparatively better osteogenesis capacity in vivo than PCL scaffolds. The aforementioned results imply that our 3D printed DCB-PCL scaffold is a promising candidate for alternative bone regeneration with a bright future as a critical bone defect treatment.

Conclusions

As a hierarchically structured composite material, bone has been a subject of research by the materials engineering community for its obvious biological value, unique structure, and mechanical properties. Our 3D printed DCB-PCL scaffolds featured macroporous structures and porosity similar to that of the trabecular bone and demonstrated promising in vitro cellular responses such as viability and osteogenic differentiation. The biogenic DCB retained many active components that are crucial for osteogenesis and bone maturing. Furthermore, as clearly demonstrated by the in vivo study, the DCB-PCL scaffold promoted bone healing and repair in the critical-sized cranial defects within a rat model. The synergistic effect of the biogenic DCB and synthetic PCL provided a strong yet porous and cell supportive platform that shows great potential for bone regeneration. In the future, this kind of attenuated immunogenicity bioactive material may be explored for its action in primates, to provide an important reference for human tissue regeneration.

Acknowledgements The authors acknowledge the financial support from National Natural Science Foundation of China (81601626), Zhejiang Provincial Natural Science of Foundation of China (Y20C070010), start-up funding from Wenzhou Institute, University of Chinese Academy of Sciences (WIUCASQD2019002) and Singapore MOE Tier 1 Grant RG46/18. The authors would also like to acknowledge the Yifan Dai's lab for providing bone tissue from alpha 1, 3 GT deficient pigs.

Author contributions H.Q. Li and L.P. Tan designed the experiments. Q.X. Pan, C.Y. Gao, Y.Y. Wang and Y.L. Wang performed the experiments. Q.X. Pan and C.Y. Gao drafted the manuscript. C. Mao, Q. Wang, F. Wen, S.N. Economidou and D. Douroumis performed the data analysis. H.Q. Li provided funding for this project and supervised the experiments. All authors edited and approved the final manuscript.

Compliance with ethical standards

Conflict of interest The authors declare that there is no conflict of interest.

Ethical approval Any related research on animal experiments included in this study is in line with ethical requirements.

References

1. Bone Grafts and Substitutes Market is Likely to Garner $3.91 Bn by 2025 (EB/OL) (2019). https://finance.yahoo.com/news/bone-grafts-substitutes-market-likely-130055628.html. Accessed 6 May 2019
2. Liu Y, Jing L, Teoh SH (2013) Review: development of clinically relevant scaffolds for vascularised bone tissue engineering. Biotechnol Adv 31(5):688–705
3. Zhang X, Awad HA, O'Keefe RJ, Guldberg RE, Schwarz EM (2008) A perspective: engineering periosteum for structural bone graft healing. Clin Orthop Relat Res 466(8):1777–1787
4. Alio del Barrio JL, Chiesa M, Garagorri N, Garcia-Urquia N, Fernandez-Delgado J, Bataille L, Rodriguez A, Arnalich-Montiel F, Zarnowski T, Alvarez de Toledo JP, Alio JL, De Miguel MP (2015) Acellular human corneal matrix sheets seeded with human adipose-derived mesenchymal stem cells integrate functionally in an experimental animal model. Exp Eye Res 132:91–100
5. Papadimitropoulos A, Scotti C, Bourgine P, Scherberich A, Martin I (2015) Engineered decellularized matrices to instruct bone regeneration processes. Bone 70:66–72
6. Magre S, Takeuchi Y, Bartosch B (2003) Xenotransplantation and pig endogenous retroviruses. Rev Med Virol 13(5):311–329

7. Sachs DH, Sykes M, Robson SC, Cooper DKC (2001) Xenotransplantation. Adv Immunol 79(11):129–223
8. Pearce AI, Richards RG, Milz S, Schneider E, Pearce SG (2007) Animal models for implant biomaterial research in bone: a review. Eur Cells Mater 13(1):1
9. Salamanca E, Lee W-F, Lin C-Y, Huang H-M, Lin C-T, Feng S-W, Chang W-J (2015) A novel porcine graft for regeneration of bone defects. Materials 8(5):2523–2536
10. Salamanca E, Hsu C-C, Huang H-M, Teng N-C, Lin C-T, Pan Y-H, Chang W-J (2018) Bone regeneration using a porcine bone substitute collagen composite in vitro and in vivo. Sci Rep 8(1):984
11. Phelps CJ, Koike C, Vaught TD, Boone J, Wells KD, Chen S-H, Ball S, Specht SM, Polejaeva IA, Monahan JA, Jobst PM, Sharma SB, Lamborn AE, Garst AS, Moore M, Demetris AJ, Rudert WA, Bottino R, Bertera S, Trucco M, Starzl TE, Dai Y, Ayares DL (2003) Production of alpha 1,3-galactosyltransferase-deficient pigs. Science 299(5605):411–414
12. Hisashi Y, Yamada K, Kuwaki K, Tseng YL, Dor FJMF, Houser SL, Robson SC, Schuurman HJ, Cooper DKC, Sachs DH, Colvin RB, Shimizu A (2008) Rejection of Cardiac Xenografts Transplanted from α1,3-Galactosyltransferase Gene-Knockout (GalT-KO) Pigs to Baboons. Am J Transpl 8(12):2516–2526
13. Cheng CW, Solorio LD, Alsberg E (2014) Decellularized tissue and cell-derived extracellular matrices as scaffolds for orthopaedic tissue engineering. Biotechnol Adv 32(2):462–484
14. Hashimoto Y, Funamoto S, Kimura T, Nam K, Fujisato T, Kishida A (2011) The effect of decellularized bone/bone marrow produced by high-hydrostatic pressurization on the osteogenic differentiation of mesenchymal stem cells. Biomaterials 32(29):7060–7067
15. Hoch AI, Mittal V, Mitra D, Vollmer N, Zikry CA, Leach JK (2016) Cell-secreted matrices perpetuate the bone-forming phenotype of differentiated mesenchymal stem cells. Biomaterials 74:178–187
16. Lu H, Hoshiba T, Kawazoe N, Koda I, Song M, Chen G (2011) Cultured cell-derived extracellular matrix scaffolds for tissue engineering. Biomaterials 32(36):9658–9666
17. Xin W, Man J, Zhou Z, Gou J, Hui D (2017) 3D printing of polymer matrix composites: a review and prospective. Compos Part B Eng 110:442–458
18. Amini AR, Laurencin CT, Nukavarapu SP (2012) Bone tissue engineering: recent advances and challenges. Crit Rev Biomed Eng 40(5):363–408
19. Trakoolwannachai V, Kheolamai P, Ummartyotin S (2019) Characterization of hydroxyapatite from eggshell waste and polycaprolactone (PCL) composite for scaffold material. Compos Part B Eng 173:106974
20. Qi X, Pei P, Zhu M, Du X, Xin C, Zhao S, Li X, Zhu Y (2017) Three dimensional printing of calcium sulfate and mesoporous bioactive glass scaffolds for improving bone regeneration in vitro and in vivo. Sci Rep 7:42556
21. Zhang J, Zhao S, Zhu Y, Huang Y, Zhu M, Tao C, Zhang C (2014) Three-dimensional printing of strontium-containing mesoporous bioactive glass scaffolds for bone regeneration. Acta Biomater 10(5):2269–2281
22. Seyednejad H, Gawlitta D, Kuiper RV, Bruin AD, Nostrum CFV, Vermonden T, Dhert WJA, Hennink WE (2012) Invivo biocompatibility and biodegradation of 3D-printed porous scaffolds based on a hydroxyl-functionalized poly(ε-caprolactone). Biomaterials 33(17):4309–4318
23. Su AP, Su HL, Wan DK (2011) Fabrication of porous polycaprolactone/hydroxyapatite (PCL/HA) blend scaffolds using a 3D plotting system for bone tissue engineering. Bioproc Biosyst Eng 34(4):505–513
24. Tarafder S, Bose S (2014) Polycaprolactone-coated 3D printed tricalcium phosphate scaffolds for bone tissue engineering: in vitro alendronate release behavior and local delivery effect on in vivo osteogenesis. ACS Appl Mater Interfaces 6(13):9955–9965
25. Saito E, Suarez-Gonzalez D, Murphy WL, Hollister SJ (2015) Biomineral coating increases bone formation by ex vivo BMP-7 gene therapy in rapid prototyped poly(l-lactic acid) (PLLA) and poly(ε-caprolactone) (PCL) porous scaffolds. Adv Healthc Mater 4(4):621–632
26. Mitsak AG, Kemppainen JM, Harris MT, Hollister SJ (2011) Effect of polycaprolactone scaffold permeability on bone regeneration in vivo. Tissue Eng PT A 17(13–14):1831
27. Pei X, Ma L, Zhang B, Sun J, Sun Y, Fan Y, Gou Z, Zhou C, Zhang X (2017) Creating hierarchical porosity hydroxyapatite scaffolds with osteoinduction by three-dimensional printing and microwave sintering. Biofabrication 9(4):045008
28. Zhang B, Sun H, Wu L, Ma L, Xing F, Kong Q, Fan Y, Zhou C, Zhang X (2019) 3D printing of calcium phosphate bioceramic with tailored biodegradation rate for skull bone tissue reconstruction. Bio Des Manuf 2(3):161–171
29. Oladapo BI, Zahedi SA, Adeoye AOM (2019) 3D printing of bone scaffolds with hybrid biomaterials. Compos Part B Eng 158:428–436
30. Mandair GS, Morris MD (2015) Contributions of Raman spectroscopy to the understanding of bone strength. Bonekey Rep 4:620
31. Taddei P, Tinti A, Reggiani M, Fagnano C (2005) In vitro mineralization of bioresorbable poly(ε-caprolactone)/apatite composites for bone tissue engineering: a vibrational and thermal investigation. J Mol Struct 744(4):135–143
32. Kister G, Cassanas G, Bergounhon M, Hoarau D, Vert M (2000) Structural characterization and hydrolytic degradation of solid copolymers of D, L-lactide-co-epsilon-caprolactone by Raman spectroscopy. Polymer 41(3):925–932
33. Zhang W, Ullah I, Shi L, Zhang Y, Ou H, Zhou J, Ullah MW, Zhang X, Li W (2019) Fabrication and characterization of porous polycaprolactone scaffold via extrusion-based cryogenic 3D printing for tissue engineering. Mater Des 180:107946
34. Lam CX, Savalani MM, Teoh SH, Hutmacher DW (2008) Dynamics of in vitro polymer degradation of polycaprolactone-based scaffolds: accelerated versus simulated physiological conditions. Biomed Mater 3(3):034108
35. Dimitriou R, Tsiridis E, Giannoudis PV (2005) Current concepts of molecular aspects of bone healing. Injury 36(12):1392–1404
36. Narayanan K, Leck KJ, Gao S, Wan AC (2009) Three-dimensional reconstituted extracellular matrix scaffolds for tissue engineering. Biomaterials 30(26):4309–4317
37. Zhao F, Kirby M, Roy A, Hu Y, Guo XE, Wang X (2018) Commonality in the microarchitecture of trabecular bone: a preliminary study. Bone 111:59–70
38. Liu F, Liu Y, Li X, Wang X, Li D, Chung S, Chen C, Lee I-S (2019) Osteogenesis of 3D printed macro-pore size biphasic calcium phosphate scaffold in rabbit calvaria. J Biomater Appl 33(9):1168–1177
39. Wu C, Luo Y, Cuniberti G, Yin X, Gelinsky M (2011) Three-dimensional printing of hierarchical and tough mesoporous bioactive glass scaffolds with a controllable pore architecture, excellent mechanical strength and mineralization ability. Acta Biomater 7(6):2644–2650
40. Millis D, Levine D (2014) Acknowledgments. In: Millis D, Levine D (eds) Canine rehabilitation and physical therapy, 2nd edn. W.B. Saunders, St. Louis
41. Ma J, Lin L, Zuo Y, Zou Q, Ren X, Li J, Li Y (2019) Modification of 3D printed PCL scaffolds by PVAc and HA to enhance cytocompatibility and osteogenesis. RSC Adv 9:5338–5346
42. Orr TE, Villars PA, Mitchell SL, Hsu HP, Spector M (2001) Compressive properties of cancellous bone defects in a rabbit model treated with particles of natural bone mineral and synthetic hydroxyapatite. Biomaterials 22(14):1953–1959

43. Beresford JN, Graves SE, Smoothy CA (2010) Formation of mineralized nodules by bone derived cells in vitro: a model of bone formation? Am J Med Genet 45(2):163–178

44. Ramaswamy Y, Wu C, Zhou H, Zreiqat H (2008) Biological response of human bone cells to zinc-modified Ca-Si-based ceramics. Acta Biomater 4(5):1487–1497

Affiliations

Qiongxi Pan[1,2] · Chenyuan Gao[2] · Yingying Wang[1] · Yili Wang[2] · Cong Mao[3] · Quan Wang[3] · Sophia N. Economidou[4] · Dennis Douroumis[5] · Feng Wen[6] · Lay Poh Tan[7] · Huaqiong Li[1,2]

[1] School of Biomedical Engineering, School of Ophthalmology and Optometry and Eye Hospital, Wenzhou Medical University, Wenzhou 325035, Zhejiang Province, People's Republic of China

[2] Engineering Research Center of Clinical Functional Materials and Diagnosis and Treatment Devices of Zhejiang Province, Wenzhou Institute, University of Chinese Academy of Sciences, Wenzhou 325011, Zhejiang Province, People's Republic of China

[3] Key Laboratory of Orthopedics of Zhejiang Province, Department of Orthopedics, The Second Affiliated Hospital and Yuying Children's Hospital of Wenzhou Medical University, Wenzhou 325027, Zhejiang Province, People's Republic of China

[4] Medway School of Pharmacy, University of Kent, Medway Campus, Central Avenue, Chatham Maritime, Chatham, Kent ME4 4TB, UK

[5] CIPER, Centre for Innovation and Process Engineering Research, Kent ME4 4TB, UK

[6] School of Chemical and Biomedical Engineering, Nanyang Technological University, Singapore 637459, Singapore

[7] School of Materials Science and Engineering, Nanyang Technological University, Singapore 639798, Singapore